Available online at www.sciencedirect.com
ScienceDirect
Journal of Power Sources 178 (2008) 445–455
JOURNAL OF POWER SOURCES
www.elsevier.com/locate/jpowsour

The study of aluminium anodes for high power density Al/air batteries with brine electrolytes

Maria Nestoridi [a], Derek Pletcher [a,*], Robert J.K. Wood [b], Shuncai Wang [b], Richard L. Jones [c], Keith R. Stokes [c], Ian Wilcock [c]

[a] *School of Chemistry, The University, Southampton SO19 1BJ, UK*
[b] *School of Engineering Sciences, The University, Southampton SO19 1BJ, UK*
[c] *dstl, Physical Sciences Department, Porton Down, Salisbury, Wilts SP4 0JQ, UK*

Received 26 October 2007; received in revised form 29 November 2007; accepted 29 November 2007
Available online 8 December 2007

Abstract

Aluminium alloys containing small additions of both tin (∼0.1 wt%) and gallium (∼0.05 wt%) are shown to dissolve anodically at high rates in sodium chloride media at room temperatures; current densities >0.2 A cm^{-2} can be obtained at potentials close to the open circuit potential, ∼−1500 mV versus SCE. The tin exists in the alloys as a second phase, typically as ∼1 μm inclusions (precipitates) distributed throughout the aluminium structure, and anodic dissolution occurs to form pits around the tin inclusions. Although the distribution of the gallium in the alloy could not be established, it is also shown to be critical in the formation of these pits as well as maintaining their activity. The stability of the alloys to open circuit corrosion and the overpotential for high rate dissolution, both critical to battery performance, are shown to depend on factors in addition to elemental composition; both heat treatment and mechanical working influence the performance of the alloy. The correlation between alloy performance and their microstructure has been investigated.

Keywords: Al alloy electrochemistry; Al dissolution; Brine-based batteries

1. Introduction

The overall goal of our programme is to develop an Al/air battery with a brine electrolyte to power a small unmanned aircraft. The specification calls for a battery weighing less than 50 g and capable of delivering an average power of 20 W and a maximum power of 34 W throughout a flight duration of 1 h in ambient conditions. This represents a substantial enhancement in performance compared to presently available Al/air batteries [1–5].

In an Al/air battery using either alkaline or brine electrolytes, the positive electrode reaction is

$$O_2 + 2H_2O + 4e^- \rightarrow 4OH^- \quad (1)$$

and the negative electrode reaction

$$Al - 3e^- \rightarrow Al(III) \quad (2)$$

and it is essential to the battery performance sought that both the Al anode and air cathode can operate at a current density ≫100 mA cm^{-2}. With a neutral brine electrolyte, the Al(III) is largely formed as a solid oxide and/or hydroxide and the performance of the battery depends critically on the form of this precipitate; it must not form a passivating film on the aluminium surface nor inhibit the air cathode. In addition, the Al material used as the negative electrode must be stable to corrosion during battery storage, i.e. the chemical reactions

$$4Al + 3O_2 + 6H_2O \rightarrow 4Al(III) + 12OH^- \quad (3)$$

$$2Al + 6H_2O \rightarrow 2Al(III) + 3H_2 + 6OH^- \quad (4)$$

should not occur during either at the open circuit potential or during anodic discharge (if all the Al is to be converted into electrical energy). It is the competing demands of stability to corrosion and rapid anodic dissolution that makes difficult the identification of appropriate aluminium alloys.

In an early study of aluminium alloys for batteries in both hydroxide and chloride media, Reding and Newport [6] surveyed several thousand alloys. More detailed investigations were ini-

* Corresponding author at: The School of Chemistry, The University, Southampton SO17 1BJ, UK. Tel.: +44 2380 593519.
E-mail address: dp1@soton.ac.uk (D. Pletcher).

0378-7753/$ – see front matter © 2008 Elsevier B.V. All rights reserved.
doi:10.1016/j.jpowsour.2007.11.108

tiated by Despic et al. [7] who investigated aluminium alloys with small additions of gallium, indium and thallium in NaCl media; they considered the influence of both composition and heat treatment on the aluminium dissolution rate and Faradaic efficiency and discuss models to relate alloy structure to their properties. The corrosion of such alloys in alkaline electrolytes at several temperatures was studied by MacDonald et al. [8] while Tuck et al. [9] reported a further study of Al–Ga alloys in both alkaline and brine media. During the 1980s, it is clear that Alcan, along with its subsidiary companies, investigated a number of multi-element alloys such as Al–Mg–Sn–Ga [2,10]; in a series of conference presentations, they reported that appropriate alloys 'activated' to give greatly enhanced rates of anodic dissolution and demonstrated superior performance in battery conditions. Indeed, a number of batteries based on these alloys have been described using both KOH [11–13] and NaCl electrolytes [14] although that with a brine electrolyte operated only at relatively low current density. More detailed reports of the electrochemistry of these alloys were, however, never published. Moreover, the past 15 years have seen relatively little extension to these studies although we would note two further papers on the dissolution of Al–In and Al–In–Ga alloys [15,16], a paper that includes studies of the corrosion of Al–Sn [17] in brine and two that discuss the cathodic activation of Al–Sn alloys [18,19].

In this paper, we describe further studies of pure aluminium and aluminium with additions of magnesium, tin and/or gallium in 2 M NaCl with a focus on defining alloys that are stable to corrosion on open circuit (i.e. during battery storage) and dissolve anodically at high rate with a high current efficiency. Relevant background information on the pitting of aluminium films and the influence of alloying elements may be found in a review by Szklarska-Smialowska [20]. The phase diagrams of the binary alloys may be found in a book [21] while there have been reports on the structure of Al–Sn alloys [22] and the influence of heat treatment on several binary alloys [23,24].

2. Experimental

Brine solutions were prepared using deionised water from a Whatman Analyst water purification system and Analytical Grade sodium chloride (Fisher Scientific). Keller's reagent (190 cm^3 H_2O + 2 cm^3 HF (48%) + 3 cm^3 HCl (36%) + 5 cm^3 HNO_3 (70%)) was prepared with high grade chemicals (Fisher Scientific).

Pure aluminium (99.999%) and nine alloys were investigated. The pure aluminium and the AlMg alloys were obtained from Goodfellow Metals. The AB50V was a preferred alloy at the end of the Alcan programme in the 1980s [10]. I0 is an alloy of similar composition prepared by Innoval Ltd. while B0–B4 were a series of alloys prepared in the Department of Metallurgy and Materials, University of Birmingham. The compositions of all these alloys are reported in Table 1. Samples of these alloys were also subjected to heat treatments as indicated in the text.

All the electrochemical experiments were carried out in a three electrode, two-compartment cell. The working electrodes were long strips of the aluminium/aluminium alloys immersed to a depth of 5 mm and having an active area of 0.25 cm^2; this simple electrode design allowed rapid removal of damaged alloy and replacement by a fresh sample for repeat experiments. For electrochemical experiments where data are reported, the Al/alloys were not polished or etched beforehand although experiments were carried out to confirm that surface preparation made little difference to the results. The counter electrode was a Pt wire in the same solution and the reference electrode was a laboratory fabricated saturated calomel electrode (SCE) with a fine porous tip and separated from the working electrode by a Luggin capillary. The tip of the Luggin capillary was placed as close as possible to the surface of the working electrode. The experiments were controlled either with a EG & G model 273 Potentiostat or a Bio-Logic model VMP2 Electrochemical Workstation and data were analysed using standard software. Open circuit potentials were measured with a Fluke 83 Multimeter. Experiments used 25 cm^3 of air-equilibrated, aqueous 2 M NaCl at room temperature (293 ± 2 K).

For electron microscopy, the strips of Al/Al alloy were mounted in epoxy resin (Struers Epofix Resin) so that only the end was exposed. The exposed surface was then (i) polished successively with 600, 1200 and 4000 grade emery paper, each for 1 min until examination of the surface by optical microscopy showed only fine scratches in the same direction (ii) polished with 6 μm diamond paste on a OP-mol cloth for 3 min (iii) repeatedly polished with 1 μm diamond paste on a DP-mol cloth for 3 min until scratches could not be seen with the optical microscope. Between each stage, the surface was washed with soap solution and then water before being dried. At the end of the preparation, the sample was cleaned with water in an ultrasonic bath. Scanning electron images were obtained with either a Jeol JSM 5910 or a Jeol FEG 6500F microscope; both allowed imaging by secondary electrons and backscattered electrons and were fitted with an Oxford Inca 300 EDX for elemental analysis. Samples for electron backscatter diffraction analysis were electropolished in 20% HNO_3 in methanol at 243 K.

3. Results

3.1. Stability to corrosion

A small sample (surface area ∼0.2 cm^2) of each of the aluminium materials were placed in ∼10 cm^3 of 2 M NaCl within a closed phial at 293 K and then observed for evidence of corrosion. The first visual sign of corrosion was the formation of small bubbles of hydrogen on the surface of the metal. This was followed by the observation of a gelatinous cloud of white precipitate (presumably alumina and/or aluminium hydroxide) around the alloy sample. With continued corrosion, the materials lost their reflective surfaces and extensive damage to the surface could be seen by scanning electron microscopy. The stability of the materials are compared in Table 1 and this table also reports the open circuit potentials measured in separate experiments (along with their elemental compositions). The pure aluminium and the alloys AlMg3 and AlMg5 (containing only additions of Mg to pure Al) quickly took up an open circuit potential close to −800 mV versus SCE and appeared to be indefinitely stable to corrosion. The alloys B1 (containing Sn but not Ga) and B3

Table 1
Composition of alloys investigated together with open circuit potentials in 2 M NaCl and observations of corrosion for alloys immersed in 2 M NaCl at 293 K

Alloy	Mg (wt%)	Sn (wt%)	Ga (wt%)	Open circuit potential (mV) vs. SCE	Observations
99.999% Al	–	–	–	−800	No evidence of corrosion over weeks
AlMg3	3	–	–	−820	No evidence of corrosion over weeks
AlMg5	5	–	–	−890	No evidence of corrosion over weeks
B0	0.5	0.1	0.05	−1530	Corrosion evident after ∼1 h
B1	0.4	0.1	–	−850	Corrosion evident after ∼1 day
B2	0.4	0.4	0.03	−1510	Corrosion evident after ∼1 h
B3	0.4	–	0.03	−800	Corrosion evident after ∼1 day
B4	–	0.1	0.03	−1500	Corrosion evident after ∼1 h
AB50V	0.6	0.1	0.05	−1530	No evidence of corrosion over weeks
I0	0.4	0.07	0.05	−1530	Corrosion evident after ∼1 h

(containing Ga but not Sn) also took up an open circuit potential close to −800 mV but showed signs of corrosion after ∼1 day. There was, however, one difference in their behaviour; the alloy B3 took up stable open circuit potential within a few seconds while the alloy B1 initially took up an initial open circuit potential of ∼−1300 mV but then drifted to −850 mV over a period of an hour. In contrast, all the alloys containing both Sn and Ga had an open circuit potential close to −1500 mV versus SCE, including one with no added Mg. These observations suggest that tin has a critical role in initiating a different mechanism for the corrosion of the aluminium materials while gallium may be important in preventing passivation once corrosion has started. While all the materials studied showed only a low rate of corrosion, it was also apparent that their stability to corrosion depended on factors additional to their nominal elemental composition. Indeed, three of the alloys (B0, AB50V and I0) have almost an identical composition (but come from different sources) but they show significant differences in their stability to corrosion. This was confirmed by examining the surfaces of the three materials using SEM after they had been exposed to a 2 M NaCl solution for a day. The image in Fig. 1(c) shows evidence of a thick film of alumina on the surface of the alloy I0 and this film is cracked and potentially porous. In strong contrast, the image of the surface of the alloy AB50V, Fig. 1(a), suggests the presence of only a very thin film of the oxide and there is no evidence of porosity. The surface of the alloy B0, Fig. 1(b), has an intermediate appearance.

The different properties of the three alloys containing both Sn and Ga and with identical compositions appears to indicate that the corrosion stability may depend on the history of the alloy including heat treatments and perhaps mechanical working. Hence, the three alloys (B0, AB50V and I0) were heated at 873 K for 2 h before being quenched by dropping into a volume of water. There was no change to the open circuit potentials in 2 M NaCl but there were marked changes to the corrosion stabilities. In fact, all three alloys showed signs of corrosion after ∼1 day, a substantial increase in corrosion resistance for B0 and I0 but a decrease in corrosion resistance for AB50V. This may imply that AB50V had already been heat treated at a lower temperature and 873 K is above the optimum temperature (see later). Certainly, the structure of the alloys and distribution of the minor elements appears to be critical in determining the properties important to battery performance.

To confirm this conclusion, samples of the alloy I0 were heat treated at 373, 473, 573, 673 K, 773 and 873 K, each for 2 h and then examined for corrosion resistance in 2 M NaCl at room temperature. The samples heated at 373–673 K all formed a fine alumina deposit within 1 h of placing them in 2 M NaCl at room temperature and the film continued to form with time. In contrast, the samples heated at higher temperature showed little sign of corrosion after 1 day and the most stable appeared to be the sample heated at 773 K which showed no change in visual appearance even after several days.

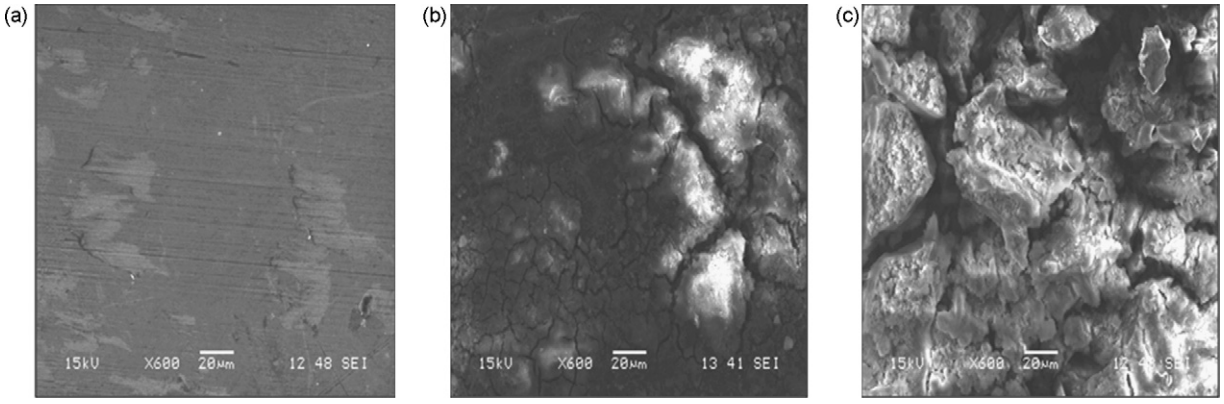

Fig. 1. SEM images of the three AlMgSnGa alloys after standing for 24 h in 2 M NaCl at room temperature. (a) AB50V (b) B0 and (c) I0.

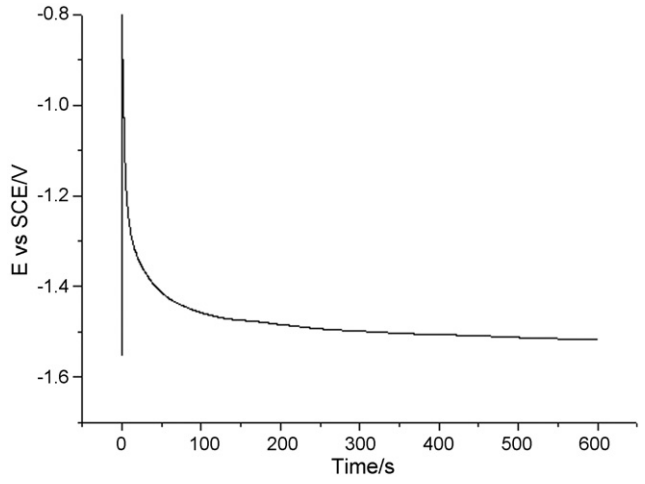

Fig. 2. Potential vs. time response to the imposition of an anodic current density of 50 mA cm^{-2} to the alloy AB50V in 2 M NaCl at room temperature.

3.2. Anodic dissolution

During preliminary experiments with the alloy AB50V in 2 M NaCl where the potential was scanned positive from −1500 mV versus SCE, it was noted that during a second scan without repolishing the alloy surface, the overpotential for aluminium dissolution was much decreased compared to the first scan. This led to the concept that the alloy could be activated by a period of anodic oxidation. Fig. 2 reports the chronopotentiometric response when an anodic current density of 50 mA cm^{-2} is applied to this alloy. It can be seen that instantaneously the potential shifts from the open circuit potential to a much less negative value and then relaxes back to a value close to the open circuit potential over a period of some 100 s. Apparently, in the steady state the alloy can dissolve at a high rate close to the open circuit potential. It will be shown below that at the end of this 'activation period', the alloy surface is highly pitted. Fig. 3 shows voltammograms on fresh and activated samples of AB50V and it can be seen that, after the anodic treatment, the voltammogram was shifted to more negative potentials by some 200 mV. While this is equivalent to a substantial improvement in battery performance, it can also be seen that the performance indicated by the data in Figs. 2 and 3 are not identical. In the constant current experiment at 50 mA cm^{-2}, the steady state potential was ∼−1530 mV while during the voltammetry, this current density was not achieved until −1290 mV. The rate of electrochemical dissolution of the aluminium alloy is clearly sensitive to the exact experiment, probably because the experiment determines the surface condition.

In consequence, the current/potential characteristics were determined in a different way. A current density of 50 mA cm^{-2} was applied to the alloy AB50V for 600s and then the current density was reduced to 1 mA cm^{-2} before being stepped to 2, 10, 50, 100, 200, 500 mA cm^{-2} at 600 s intervals. At each current density, the potential was monitored. Fig. 4 shows a typical set of data while the inset reports the resulting current density versus potential characteristic. It can be seen that a dissolution rate of 0.1 A cm^{-2} was possible at a potential of −1440 mV versus SCE, only 90 mV positive to the open circuit potential. Higher dissolution rates were also possible although the potentials measured become increasingly unreliable because of both uncorrected IR drop and changes to the alloy sample during the experiment. During the period of 600 s at each potential and particularly at the higher current densities, a substantial fraction of the Al alloy sample dissolved anodically (as shown by Faraday's law calculations and visual observation) and, in addition, considerable oxide in the electrolyte could be seen. In consequence, the surface of the alloy must have changed dramatically during the experiment and, for example, the real surface area will have become ill-defined. To some extent, the influence of such factors could be avoided by using fresh samples of alloy for each current density and applying the higher current density immediately after the activation pulse. Indeed, this approach was used for some of the data in Table 2. Overall, it is clear that the

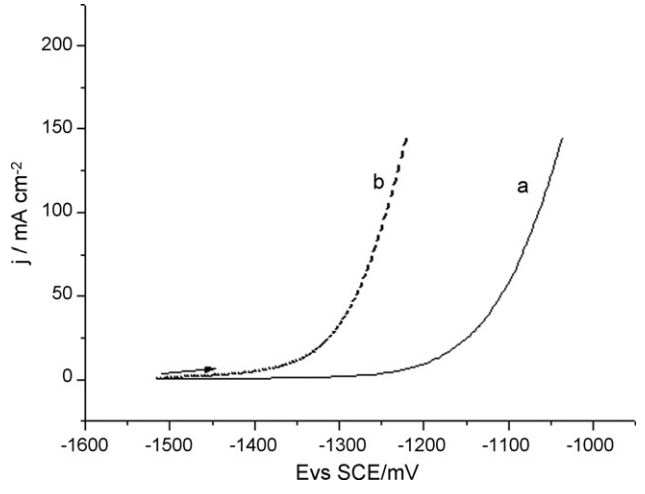

Fig. 3. Voltammograms for the alloy AB50V in 2 M NaCl (a) before and (b) after activation by the imposition of an anodic current density of 50 mA cm^{-2} for 600 s.

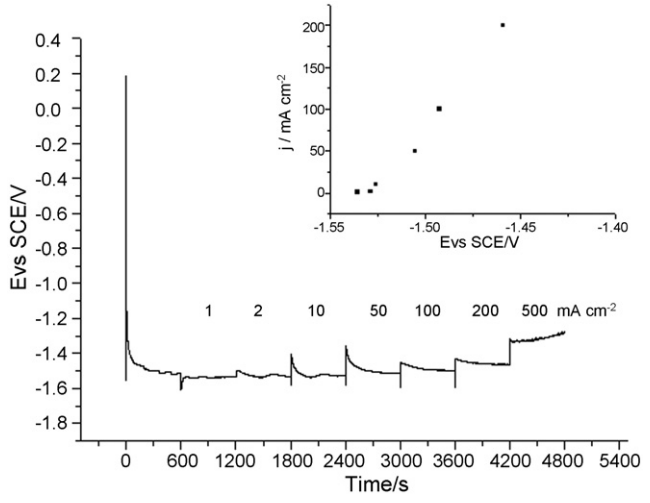

Fig. 4. Potential vs. time response for the alloy AB50V in 2 M NaCl in an experiment where (a) the surface was activated by the imposition of an anodic current density of 50 mA cm^{-2} for 600 s (b) the anodic current densities was stepped to 1, 2, 10, 50, 100, 200 and 500 mA cm^{-2} at 600 s intervals. The inset shows the resulting j vs. E characteristic.

Table 2
Current density/potential characteristics for the alloys in 2 M NaCl at 293 K

Alloy	Potential vs. SCE (mV)					
	1 mA cm^{-2}	4 mA cm^{-2}	10 mA cm^{-2}	50 mA cm^{-2}	100 mA cm^{-2}	200 mA cm^{-2}
99.999% Al	−775	−770	−750	−660	−530	−230
B0	−1540	−1520	−1480	−1450	−1440	−1390
B1	−860	−800	−790	−770	−740	−680
B2	−1530	−1490	−1440	−1380	−1260	−1120
B3	−810	−790	−760	−720	−700	−620
B4	−1530	−1520	−1510	−1500	−1490	−1460
AB50V	−1540	−1530	−1510	−1470	−1440	−1380
I0	−1540	−1530	−1500	−1490	−1480	−1450
Heated to 873 K for 2 h						
B0	−1530	−1520	−1490	−1480	−1460	−1390
AB50V	−1530	−1520	−1500	−1490	−1470	−1400
I0	−1550	−1530	−1500	−1490	−1480	−1450

Data obtained potentiometrically (current varied at 600 s intervals) following activation at 50 mA cm^{-2} for 600 s.

alloy AB50V could be dissolved at very high rates, >0.2 A cm^{-2}, close (i.e. within 200 mV) to the open circuit potential. In further experiments, it was also shown that the alloy AB50V could be activated with an anodic current in brines containing 0.2 M to saturated NaCl and the activation time decreased with increasing current density. In all the solutions, high steady state current densities could be achieved close to −1500 mV versus SCE.

The current/potential characteristics for a series of the alloys in 2 M NaCl were determined using the controlled current technique following activation with an anodic current density of 50 mA cm^{-2} and the data are reported in Table 2. Pure aluminium and the alloys B1 and B3 did not show a negative potential shift during the passage of 50 mA cm^{-2} and at all current densities, the potential was positive to −800 mV. All the other alloys examined showed a negative shift in potential to ∼−1500 mV versus SCE during the initial 600 s polarisation at a current density of 50 mA cm^{-2} and dissolved at high rates close to the open circuit potential. It should be noted that the three alloys with the same elemental composition (B0, AB50V and I0) had similar current/potential characteristics. The alloy B2 (high Sn) showed poorer performance at high current densities. While the alloy B4 (no Mg) gave similar current/potential data in Table 2 to other alloys containing Sn and Ga, at very high current densities, it could be seen by eye to show a significantly higher level of physical disintegration. Hence, the magnesium does appear to have a beneficial role in the battery material.

Table 2 also reports the current/potential characteristics for the three alloys with the same elemental composition (B0, AB50V and I0) after a heat treatment. The heat treatment at 873 K for 2 h leads to a small negative shift in the potentials at all current densities for each of the alloys. To further define the influence of heat treatment, samples of the alloy I0 were heated at a series of temperatures between 373 K and 873 K for 2 h. The samples were then activated with an anodic current density of 50 mA cm^{-2} for 600 s before a current/potential characteristic was recorded using the stepped current procedure. With all samples, small negative shifts in potential were observed at each current density. The data is illustrated in Fig. 5 by the potentials with a current density of 120 mA cm^{-2} for the alloy I0. Although the differences are small, it would appear that the optimum temperature for the heat treatment is 573 K. These results are discussed further later in the paper.

3.3. Microstructural studies

The results in Section 3.2 clearly confirm that alloys containing Mg, Sn and Ga are capable of electrochemical dissolution at the high rates necessary to serve as the negative electrode in a high power density aluminium/air battery with a sodium chloride electrolyte [2,10,14]. Indeed, the greatest difference between the materials was in their stability to open circuit corrosion, as described in Section 3.1, and this is relevant to battery performance particularly if the batteries are to be stored filled with electrolyte. In this section, a number of microstructural studies were carried out with the objectives of understanding the mechanism by which (a) the alloying elements Sn and Ga combine to promote rapid anodic dissolution and (b) the open circuit corrosion rate varied with alloy fabrication.

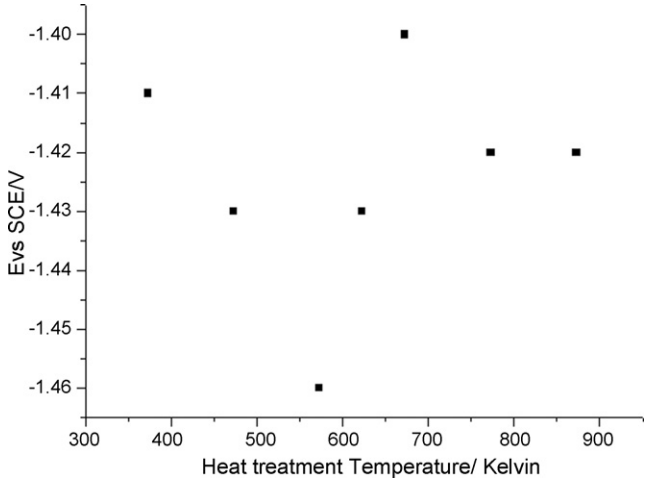

Fig. 5. Influence of the temperature for heat treatment on the potential observed when the alloy I0 was dissolved employing a current density of 120 mA cm^{-2}. 2 m NaCl. Room temperature. Heat treatment time 2 h.

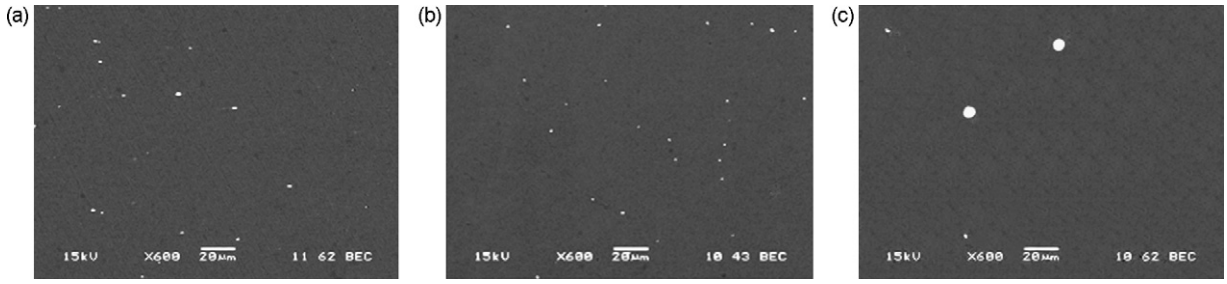

Fig. 6. SEM images, using the backscatter electron detector, of the three alloys after polishing. (a) AB50V (b) B0 (c) I0. The white spots are the tin inclusions.

Scanning electron micrographs were recorded for polished samples of AB50V, B0, and I0 using the backscatter electron detector in order to define the distribution of the higher atomic number elements in the alloys. With all three alloys, the images showed bright spots, distributed over the whole surface, see Fig. 6, and EDAX confirmed that tin was a major component of these particles. Some of the particles also contained magnesium. Hence, it is confirmed that the tin is largely present in the alloys as small inclusions, i.e. as separate phases within the main aluminium structure; the Al–Sn phase diagram shows that tin is poorly soluble in aluminium and it is therefore expected to precipitate as a different phase during preparation of the alloys. With the alloys AB50V and B0, the tin particles were quite uniform in size, typically ∼1 μm and scattered across the whole surface. With the alloy I0, however, there were fewer tin inclusions less uniformly scattered across the surface and some of the inclusions are significantly larger, ∼8 μm. This conclusion could be confirmed by etching the alloys in Keller's reagent for 10 s. This etching procedure led to a surface with rounded pits where tin inclusions could be seen within many of the pits; Fig. 7 illustrates such a surface (in fact, for AB50V). The etched surfaces of AB50V and B0 appeared similar but the surface of I0 showed many fewer but much larger pits. In contrast, a similar etch of pure aluminium did not lead to pitting while etching of B1 (no gallium) led to pits with a different form—the pits were more angular and seldom associated with a tin inclusion. Unlike tin, it was not possible to locate the gallium, either before or after etching but this is not surprising since it is present at very low levels in all the alloys.

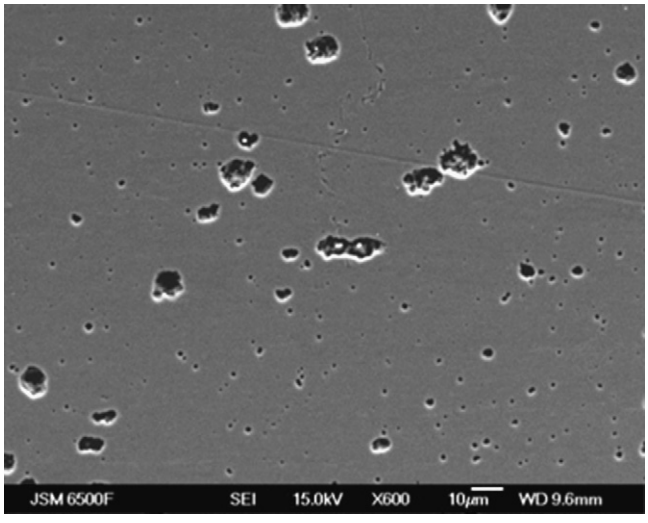

Fig. 7. SEM image using the backscatter electron detector of the alloy AB50V after etching a polished surface with Keller's reagent.

Fig. 8 shows SEM images of the surface of the alloy AB50V after it had been subjected to an anodic current density of 50 mA cm^{-2} for 10 s. The low magnification image, Fig. 8(a) shows that the passage of only 0.5 C cm^{-2} has led to extensive surface damage and that a large number of rounded pits have been formed. Fig. 8(b) and (c) show higher magnification images together with EDAX analysis at various points on the surface. The pits are again rounded and the EDAX mapping of the low magnification image shows that a large fraction of the pits contain a Sn or SnMg inclusion. The others are large enough to postulate that a tin inclusion had been physically lost during the expansion of the pit. Indeed, the distribution of the pits appears to reflect the distribution of the tin inclusions. It appears that the facile dissolution of the aluminium at potentials close to −1500 mV versus SCE is associated with the formation of the rounded pits and, again, the tin inclusions have a key role in the formation of these pits. The highest magnification image, Fig. 8(c), shows a typical 'dissolution centre'; it can be seen to be large enough to consist of overlapping pits and each of the pits is around a Sn inclusion. In further experiments, it was confirmed that the number and the size of the pits increased with both the dissolution current density and dissolution time. Also similar images could be obtained with B0 and I0 and also by etching any of the three alloys in Keller's reagent. Hence, it appears that the Sn inclusions are critical to the mechanism promoting a high rate of dissolution with alloys that support dissolution close to −1500 mV versus SCE.

Again, the EDAX did not identify the presence of gallium and hence direct evidence for its role could therefore not be determined. Hence, an indirect approach had to be employed. The alloy B1, containing Mg and Sn but not Ga, was subjected to the passage of an anodic current density of 50 mA cm^{-2} for 10 s. Since the charge passed is 0.5 C cm^{-2}, the same as that employed above for the anodic dissolution of the alloys containing both Sn and Ga, substantial surface damage or oxide formation must again be expected. With B1, however, the potential during oxidation remained ∼−800 mV, i.e. a much higher overpotential was necessary to form the pits in B1 than in the alloys containing both Sn and Ga. Fig. 9 shows SEM images of the surface of the alloy B1 after the period of anodic dissolution. It can be seen that the pits in the surface of B1 are angular,

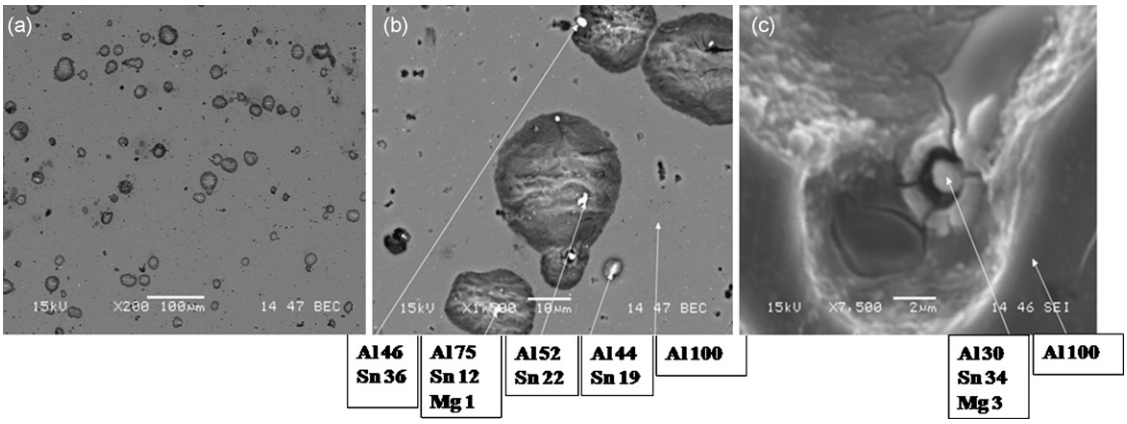

Fig. 8. SEM images of the surface of the alloy AB50V after the passage of a current density of 50 mA cm^{-2} for 10 s. (a) Low magnification image, (b) medium magnification image with EDAX analysis at selected points and (c) high magnification image with EDAX analysis at selected points. The EDAX analyses are shown as atomic %—only the metal components are shown.

not rounded; rather the pit morphology is crystallographic in nature and there are many linked cavities. This pattern is very similar to that reported recently for AlFe alloys [24]. A similar oxidation charge with pure aluminium also led to angular pits although with a lower number density suggesting that oxide film formation is a more important reaction in the absence of alloying elements. Moreover, a higher magnification image of a pit in B1, Fig. 9(a) suggests that the aluminium oxide/hydroxide within the pit has a more crusty appearance than observed for the AlMgSnGa alloys. In addition, in contrast to the experiments with AB50V, B0 and I0, an SEM image using the backscatter electron detector revealed (a) no evidence that the pits were associated with Sn inclusions and (b) many Sn inclusions remained dormant. These differences certainly imply that the gallium has a role in activating the tin inclusions for pit formation. The gallium may also be important in preventing passivation by alumina leading to termination of pit growth.

The as-received conditions of three alloys with the similar composition (AB50V, B0 and I0) were examined by electron backscatter diffraction (EBSD) in SEM. Fig. 10 shows the grain boundary maps, the grain orientation maps and the {1 1 1} pole figures [25,26] for the three alloys. The shades in the grain orientation maps represent different orientations of the grains and hence discloses the grain sizes. In the grain boundary maps, the dark and grey lines represent misorientation angles >15° (i.e. High Angle Grain Boundaries or HAGB) and 2–15° (i.e. Low Angle Grain Boundaries or LAGBs), respectively. Clearly, the grain boundary maps are also indicative of grain size. For the alloys of interest, the grain sizes in the three alloys (with the same elemental composition) are significantly different. Both B0 and I0 consist of large grains separated by HAGBs with these large grains containing relatively few LAGBs. The pattern for AB50V is quite different. It has much smaller, band like grains and there is an intricate pattern of grain boundaries, both HAGBs and LAGBs. This is the pattern expected for an alloy that has been cold worked, probably by rolling. These conclusions are confirmed by the {1 1 1} pole figures. That for AB50V shows a typical rolled structure with mixtures of three textures: {1 1 2}⟨1 1 1⟩, {1 2 3}⟨6 3 4⟩, and {0 1 1}⟨2 1 1⟩ as was expected. In contrast, those for B0 and I0 show a random distribution of the grains; the only difference between (iii) b and (iii) c in Fig. 10 is that the grains are more dense in (iii) b and this is consistent with a smaller grain size for B0 than I0.

Electron backscatter diffraction (EBSD) was also used to probe the influence of heat treatment on the alloys. In the first experiment, the grain boundary and orientation maps were col-

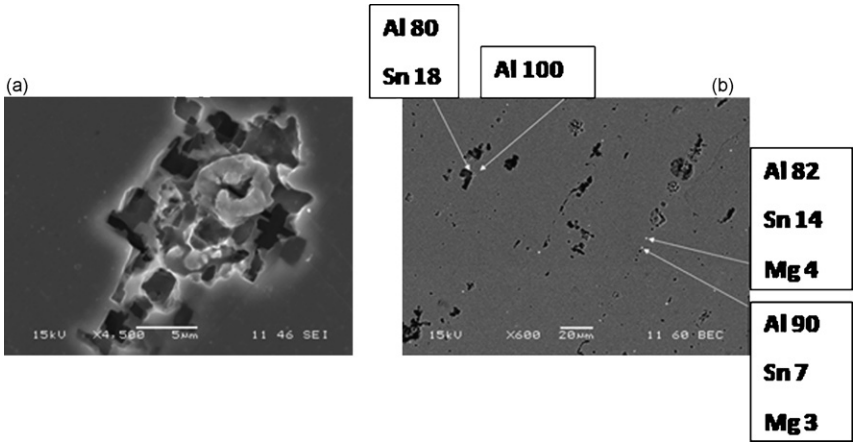

Fig. 9. SEM images of the surface of the alloy B1 after the passage of 50 mA cm^{-2} for 10 s. (a) Secondary electron detector and (b) backscatter electron detector with EDAX analysis at selected points. The EDAX analyses are shown as atomic %—only the metal components are shown.

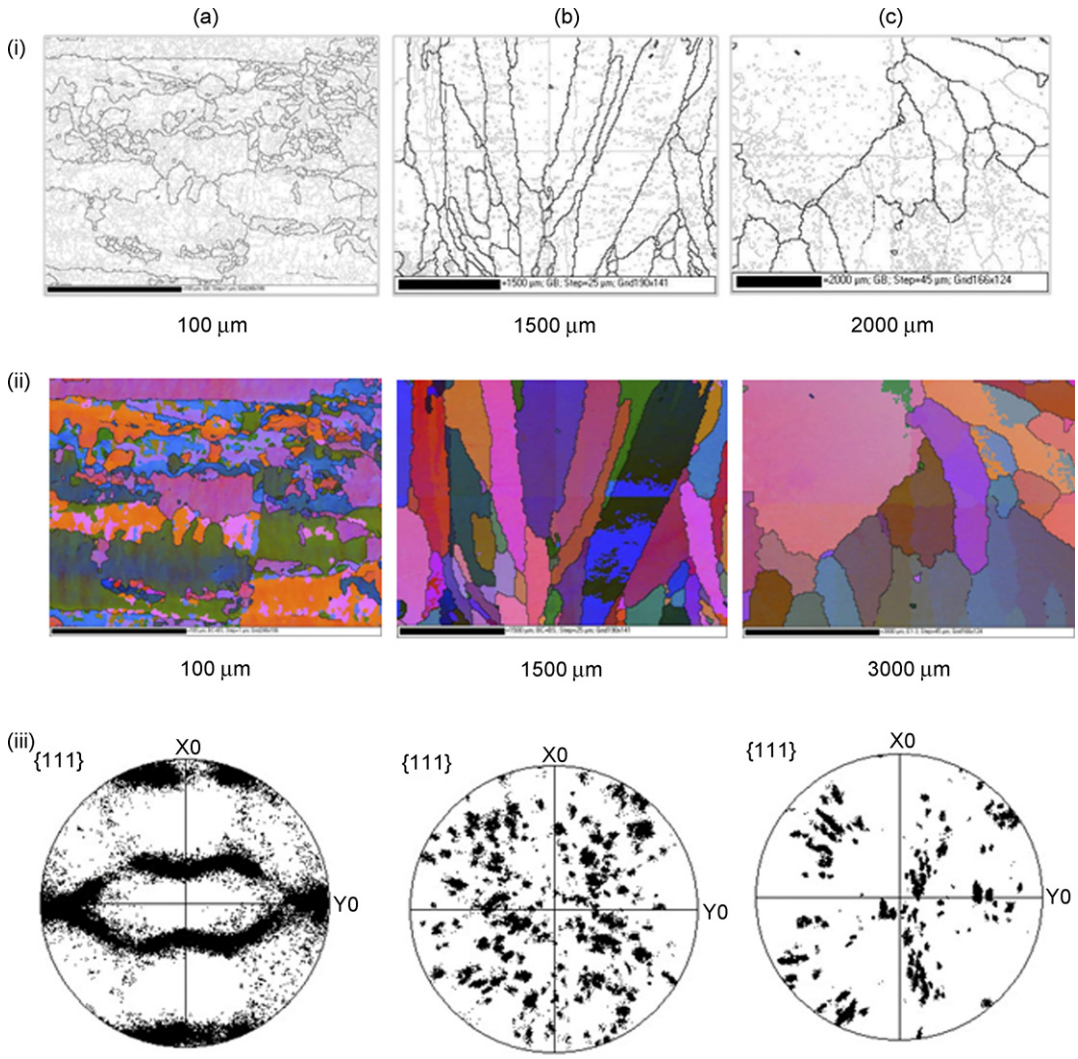

Fig. 10. EBSD analysis (i) grain boundary map (ii) orientation maps (iii) corresponding {1 1 1} pole figures for (a) AB50V (b) B0 and (c) I0—note different scale bars.

lected for a sample of the alloy I0 before and after heat treatment at 573 K for 2 h. The maps were remarkably similar confirming that the grain size and orientation were not changed by the heat treatment. Since the alloy I0 was in the as-cast condition and had not been cold worked, this is to be expected [25]. It was, however noted above, see Fig. 5, that the dissolution of aluminium occurred at lower overpotential after heat treatment. One can only speculate that this improvement in performance is due to a redistribution of a minor element, most likely gallium, leading to higher concentration at the dissolution sites that enhances the kinetics of aluminium oxidation or modifies the properties of the oxide film at these locations.

With AB50V, the influence of heat treatment on alloy structure was more interesting. Samples were heat treated at 573 and 873 K for 2 h and analysed by EBSD. Fig. 11 compares the grain boundary maps, the grain orientation maps and the {1 1 1} pole figures for the heat treated samples with the as-received sample. It can be seen that after the heat treatment at 573 K, the rolling textures have degraded to some extent. After heat treatment at 873 K, major changes have occurred. The pole figure indicates a scattered cubic structure of $\{1\,0\,0\}\langle 0\,0\,1\rangle$. Even at 573 K, the grain boundary and orientation maps indicate that the grains are bigger than in the as-received alloy and most of the grain boundaries are HAGBs. After heat treatment at 873 K, the grain orientation map shows less contrast in shades and the grain boundary map, by and large, shows only a network of LAGBs. The sample is tending towards a single grain at 873 K. This is also consistent with the pole figure. A recent paper reports similar changes in structure for a AlMg alloy [27] while the literature [28] confirms that cold working is a necessary prerequisite to structure changes during heat treatment.

Overall, it may be concluded that, within the limited number of materials examined, there is a correlation between the structure of these AlMgSnGa alloys and their resistance to corrosion; the band like, small grained structure resulting from rolling without heat treatment seems to give the lowest corrosion rate.

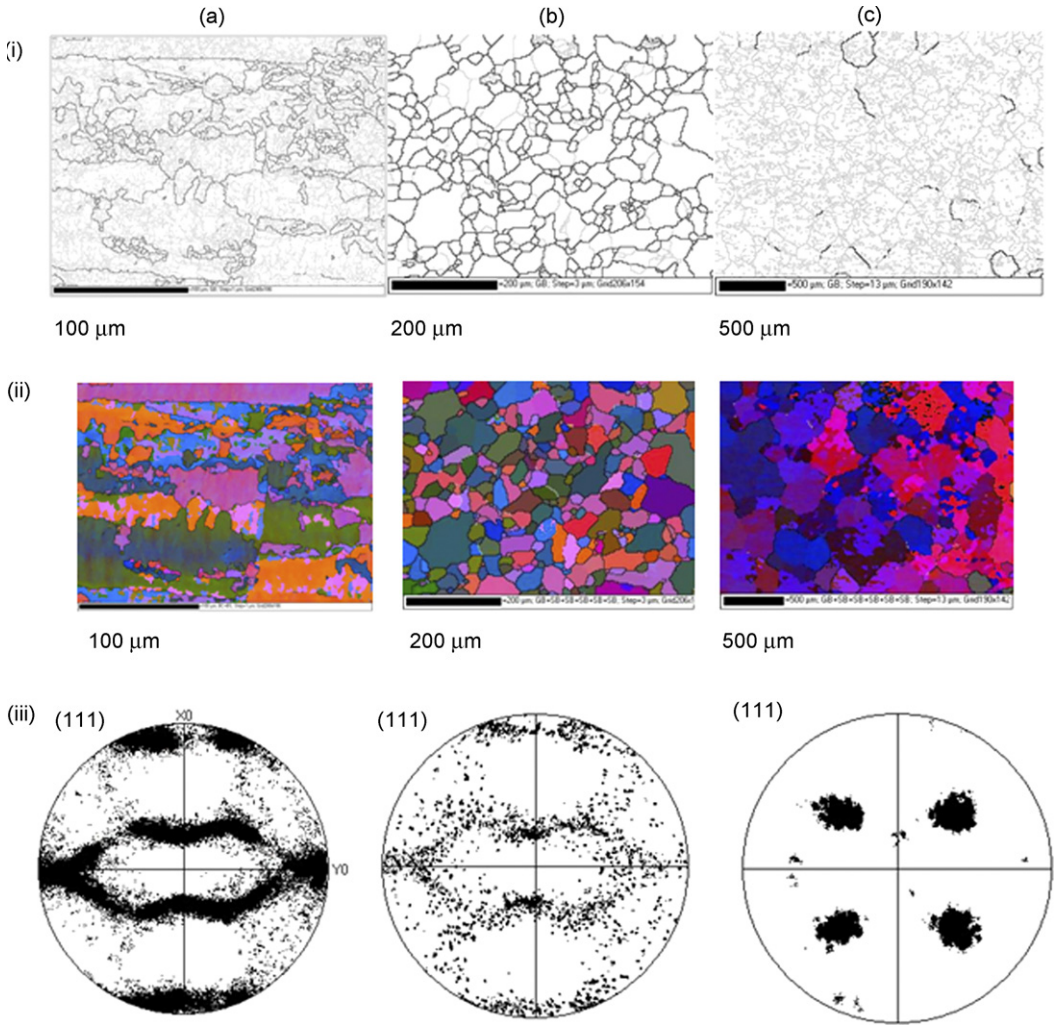

Fig. 11. EBSD analysis (i) grain boundary map (ii) orientation maps (iii) corresponding {1 1 1} pole figures for AB50V (a) as received (b) heat treated for 2 h at 573 K and quenched (c) heat treated for 2 h at 873 K and quenched—note different scale bars.

4. Discussion

There is strong evidence that the presence of both Sn and Ga in the alloy facilitates a new mechanism for the dissolution of aluminium in the brine medium at room temperature. This is clear from the shift in the potential for dissolution from ∼−800 mV in the absence of both elements to ∼−1500 mV when both are present. In addition, the morphology of the pitting changes with this shift in dissolution potential. The pits become rounded and centred around the tin inclusions.

In the chemical etching of the alloys, it is relatively easy to envisage a role for the tin inclusions—tin is far superior to aluminium as a catalyst for hydrogen evolution [29] and it is to be expected that the tin inclusions will act as cathodic centres during the corrosion process. In the anodic dissolution reaction, the need for cathodic centres does not arise and the role of the tin cannot be the same in steady state anodic dissolution as that occurring during corrosion. There remains, however, the possibility that a 'corrosion mechanism' is involved in the initiation of the pit formation and consequent Al dissolution, thereby fixing the site of later dissolution; we therefore plan attempts to use optical microscopy to observe pit formation during the initial stages of the dissolution to see whether hydrogen gas is formed.

The distribution of the gallium in the alloys could not be determined during this investigation but this element, present in low amounts, has an essential role in the low overpotential Al dissolution process. Gallium has a very low melting point, 303 K, and is therefore likely to be very mobile within the alloy structure even at room temperature while the Al–Ga phase diagram reveals no intermetallic compounds and very limited mutual solubilities. Moreover, several recent papers have shown that liquid gallium decorates the grain boundaries in polycrystalline aluminium and confirm that this is a rapid process [30–33]. Hence, it is to be expected that the gallium accumulates in the grain boundaries along with the tin inclusions. With another relatively low melting point metal, lead, it was certainly found that heat treatment of AlPb alloys close to the melting point of lead leads to accumulation of the lead at the surface [34,35]. The same authors conclude that Mg increases the movement of the Pb within the alloy structure. Similar accumulation of gallium at the surface of the AlMgSnGa alloys could have a significant influence on the electrochemistry of the system. Particularly mixed with

other metals, even at room temperature the gallium could form a 'liquid-like' film within the grain boundaries and this would have similar properties to amalgam films, i.e. much enhanced rates of electron transfer and a substantially reduced tendency to form passivating films.

It is also possible that both Sn and Ga activate the alloys to anodic dissolution via their influence on the properties of the alumina film on the alloy surface. This could either be the result of Sn or Ga permitting the pitting of the native alumina layer present before the dissolution is commenced and certainly, the Sn within this alumina layer is likely to reflect the distribution of the tin inclusions within the alloy. Equally, the elements could locally prevent the repassivation by an alumina layer after dissolution has commenced.

It has also been found that alloys with the same elemental composition from different sources show different properties probably because of mechanical working or different temperatures of preparation and/or cooling regimes as well as post-heat treatments. In particular while the overpotentials for Al dissolution are similar, there is a marked difference in their stability to corrosion on open circuit. The alloy, AB50V, with the smallest grain size showed the greatest stability and this is contrary to conventional wisdom. It was, however, concluded that this alloy had been subjected to cold rolling and perhaps a low temperature heat treatment and it was also found that some heat treatments of the alloy, I0, increased its stability to corrosion and also led to a decrease in overpotential for Al dissolution. The differences in the alloy properties could, however, also result from differences in the temperature of mixing of the metals during alloy preparation or differences in cooling regimes. Certainly, in view of the results with AlPb alloys [34,35], the heat treatments used would be expected to lead to diffusion of Ga into the intergranular boundaries and this may be critical to the corrosion resistance. The experiments with I0 showed that the grain size did not change with temperature.

The EBSD studies on the heat treated AB50V confirmed that there was a correlation between the grain structure and stability to corrosion with the band like, small grained structure resulting from rolling giving the best performance. It would be interesting to see whether similar correlation exist with related alloys.

Unfortunately, in all programmes where low levels of alloying elements are being investigated, it is always possible that trace contaminants determine the results. This study cannot escape this difficulty. Hence, in considering the difference in the behaviour of the three alloys with the same nominal composition, a role for very minor contaminants such as iron cannot be ruled out. Such impurities could well be below the lowest elemental detection limit and arise either from an impurity in the aluminium starting material or contamination during alloy preparation or processing. Low levels of such metals could influence the electrochemistry and corrosion resistance of the alloys; after all, it is a conclusion of this paper that a low level of gallium has a large influence on the electrochemistry of the alloys. Since the contaminants are likely to be in the grain boundaries, their level in the grain boundaries should correlate with grain size. Indeed, with the alloys, AB50V, B0 and I0, their stability to corrosion decreases with increasing grain size.

We believe that each of the alloys AB50V, B0 and I0, as well as related compositions are likely to be suitable anodes for a high power density aluminium/air battery. We would, however, recommend that the anode alloy should contain Mg, Sn and Ga and be prepared from the highest purity metals. For a battery to be stored containing electrolyte, we believe that the alloy should be rolled but not subjected to heat treatment.

Acknowledgements

The authors would like to thank Dr. David Fort (University of Birmingham) for the preparation of the alloys B0–B4 and Dr. Clive Tuck for advice. They also wish to acknowledge MoD for the financial support of this programme.

References

[1] J.P. Induce de Souza, W. Vielstich, in: W. Vielstich, H.A. Gasteiger, A. Lamm (Eds.), Handbook of Fuel Cells—Fundamentals, Technology and Applications, vol. 1, John Wiley, 2003, Chapter 23.
[2] C.D.S. Tuck, Modern Batteries, Ellis Horwood, 1991, p. 487.
[3] R.P. Hamlen, T.B. Atwater, in: D. Linden, T.B. Reddy (Eds.), Handbook of Batteries, 3rd ed., McGraw Hill, 2002, Chapter 38.
[4] E.J. Rudd, D.W. Gibbons, J. Power Sources 47 (1994) 329.
[5] Q. Li, N.J. Bjerrum, J. Power Sources 110 (2002) 1.
[6] J.T. Reding, J.J. Newport, Mater. Prot. 5 (1966) 15.
[7] A.R. Despic, D.M. Drazic, M.M. Purenovic, N. Cikovic, J. Appl. Electrochem. 6 (1976) 527.
[8] (a) D.D. MacDonald, S. Real, M. Urquidi-MacDonald, J. Electrochem. Soc. 135 (1988) 2397;
(b) D.D. MacDonald, S. Real, M. Urquidi-MacDonald, J. Electrochem. Soc. 135 (1988) 1633.
[9] C.D.S. Tuck, J.A. Hunter, G.M. Scamans, J. Electrochem. Soc. 134 (1987) 2970.
[10] J.A. Hunter, G.M. Scamans, J. Sykes, Int. Power Symp. 17 (1993) 193.
[11] G.M. Scamans, J.A. Hunter, C.D.S. Tuck, R.P. Hamlen, N.P. Fitzpatrick, Int. Power Symp. 12 (1988) 363.
[12] W.B. O'Callaghan, N.P. Fitzpatrick, K. Peters, Proceedings of the 11th International Telecommunications Energy Conference, Firenze, Italy, 1989.
[13] G.M. Scamans, S.M. Warner, Proceedings of the 6th Battery Conference and Exhibition, ERA Technology, London, 1990.
[14] E. Budevski, I. Iliev, A. Kaisheva, A. Despic, K. Krsmanovic, J. Appl. Electrochem. 19 (1989) 323.
[15] S. Zein El Abedin, A.O. Saleh, J. Appl. Electrochem. 34 (2004) 331.
[16] S. Zein El Abedin, F. Endres, J. Appl. Electrochem. 34 (2004) 1071.
[17] J.T.B. Gundersen, A. Aytac, J.H. Nordlien, K. Nisancioglu, Corros. Sci. 46 (2004) 697.
[18] M. Kliskic, J. Radosevic, S. Gudic, M. Smith, Electrochim. Acta 43 (1998) 3241.
[19] S. Gudic, J. Radosevic, I. Smoljko, M. Kliskic, Electrochim. Acta 50 (2005) 5624.
[20] Z. Szklarska-Smialowska, Corros. Sci. 41 (1999) 1743.
[21] J.R. Davis (Ed.), Aluminium Aluminium Alloys, AST International, 1993.
[22] S. Abis, G. Barucca, P. Mengucci, J. Alloys Compd. 215 (1994) 309.
[23] J.T.B. Gundersen, A. Aytaç, J.H. Nordlien, K. Nişancioğlu, Corros. Sci. 46 (2004) 697.
[24] R. Ambat, A.J. Davenport, G.M. Scamans, A. Afseth, Corros. Sci. 48 (2006) 3455.
[25] P.J. Goodhew, J. Humphreys, R. Beanland, Electron Microscopy and Analysis, Taylor and Francis, 2001.
[26] M.J. Starink, S.C. Wang, N. Gao, H. Singh Ubhi, C. Xu, T.G. Langdon, Mater. Sci. Forum 503 (2006) 937.
[27] P.J. Hurley, F.J. Humphreys, J. Microsc. 213 (2004) 225.

[28] W.D. Callister, Materials Science and Engineering—An Introduction, John Wiley, 2007, p. 721.
[29] S. Trasatti, J. Electroanal. Chem. 39 (1972) 163.
[30] R.C. Hugo, R.G. Hoagland, Scipta Mater. 41 (1999)1341.
[31] J. Hagström, O.V. Mishin, B. Hutchinson, Scipta Mater. 49 (2003)1035.
[32] T. Ohgaki, H. Toda, I. Sinclair, J.-Y. Buffière, W. Ludwig, T. Kobayashi, M. Niinomi, T. Akahori, Mater. Sci. Eng. A 427 (2006) 1.
[33] M. Kobayashi, H. Toda, K. Uesugi, T. Ohgaki, T. Kobayashi, Y. Takayama, B.-G. Ahn, Phil. Mag. 86 (2006) 4351.
[34] Y.W. Keuong, J.H. Nordlien, S. Ono, K. Nisancioglu, J. Electrochem. Soc. 150 (2003) B547.
[35] Y. Yu, O. Saevik, J.H. Nordlien, K. Nisancioglu, J. Electrochem. Soc. 152 (2005) B327.